A new depositional model for the classical turbidite locality at San Clemente State Beach, California

Hilario Camacho, Cathy J. Busby, and Ben Kneller

ABSTRACT

The Miocene turbidite system exposed in the beach cliffs at San Clemente State Beach, California, has been used by industry and academia alike as a field laboratory. It has been used as an analog for petroleum reservoirs in the Los Angeles Basin and other areas. We interpret the turbidite system at San Clemente State Beach to represent the fill of a single turbidite channel that aggraded subvertically. This interpretation is based on construction of a detailed photomosaic, mapping of three-dimensional facies distributions, measurement of representative sections, and collection of new paleocurrent data; we also extended this analysis to outcrops not previously described in the literature. The channel had a minimum width of 1 km and a paleotransport direction toward the northwest. Our new paleocurrent measurements indicate an average transport direction of 321° for the channel deposits, approximately perpendicular to previously published paleocurrent data. Our paleocurrent data are in agreement with the trend of the channel as defined by facies mapping. The lateral and vertical facies changes along the sea cliffs at San Clemente are a result of interfingering between axial and marginal facies within a single turbidite channel. We interpret the turbidite channel to have been cut into a low-gradient continental slope (less than 1°), rather than representing a channel on a submarine fan. We propose that the Gollum channel system is a modern analog of the turbidite system at San Clemente State Beach.

INTRODUCTION

The turbidite system exposed on the sea cliffs at San Clemente State Beach, California, has been used by industry and academia alike as a field laboratory and an analog for unpublished studies of subsurface turbidite reservoirs. The sedimentary section at San

Manuscript received March 13, 2000; revised manuscript received August 6, 2001; final acceptance March 18, 2002.

AUTHORS

HILARIO CAMACHO ~ *Department of Geological Sciences, University of California, Santa Barbara, Building 526, Santa Barbara, California, 93106; camacho@geol.ucsb.edu*

Hilario Camacho received a B.Sc. degree in geology from the Universidad de Granada, Spain, in 1992 and an M.S. degree from California State University, Long Beach. He is currently a Ph.D. candidate at the University of California, Santa Barbara, and is chief geologist at Signal Hill Petroleum, Inc., in Long Beach, California. His research interests are focused on fluid flow in sedimentary basins, oil generation and migration, and siliciclastic diagenesis.

CATHY J. BUSBY ~ *Department of Geological Sciences, University of California, Santa Barbara, Building 526, Santa Barbara, California, 93106; cathy@geol.ucsb.edu*

Cathy Busby received her B.S. degree from the University of California at Berkeley in 1977 and her Ph.D. from Princeton University in 1983. She then joined the faculty at the University of California at Santa Barbara, where she has been a professor since 1992. As part of her research on the tectonics of sedimentary basins, she has published on turbidite facies architecture in outcrop, making comparisons with modern analogs and subsurface examples. She teaches turbidite courses at the graduate level and for industry.

BEN KNELLER ~ *Institute for Crustal Studies, 1140 Giruetz Hall, University of California, Santa Barbara, California, 93106; ben@crustal.ucsb.edu*

Ben Kneller gained his B.Sc. degree from the University of Sheffield and his Ph.D. from the University of Aberdeen, United Kingdom. He was formerly on the faculty at the University of Leeds, where he initiated and, for seven years, led the Turbidites Research Group. He is now a researcher at the University of California at Santa Barbara. He has applied a combination of traditional facies-based field studies, experimental work, and theory to turbidite process sedimentology. He regularly consults and teaches short courses for industry.

ACKNOWLEDGEMENTS

This work was funded by grant number PRF 32624-AC8 from the American Chemical Society to Cathy Busby and by a gift from ARCO to Cathy Busby. Additional support from Signal Hill Petroleum, Inc., to Hilario Camacho is also acknowledged. The article was greatly improved by the comments of William Morris and the formal reviewers W. Normark and J. Coleman. Thanks to Kari Bassett for assisting Cathy Busby in shooting the photomosaic and making the earliest line drawings. Discussions in the field at San Clemente with Jeff Peakall are gratefully acknowledged.

Clemente State Beach (Figure 1) consists of coarse-grained to fine-grained sandstones, siltstones, and mudstones, as well as lesser conglomerates. These upper Miocene–lower Pliocene deposits (Ingle, 1971) were informally referred to by Weser (1971) as the San Clemente lens of the Capistrano Formation. Foraminifera assemblages from the Capistrano Formation around the Dana Point area indicate midbathyal paleowater depths of approximately 2000–3000 m (Ingle, 1971).

Several previous studies have proposed depositional models for the sedimentary sequence at San Clemente (Weser, 1971; Walker, 1975; Hess, 1979; Clark and Pickering, 1996). All of these authors interpreted the turbidite system at San Clemente to record deposition in a deep-sea fan environment. These studies focused on the analysis of vertical trends (one-dimensional [1-D] analysis) and on the two-dimensional (2-D) lateral facies distribution along the outcrop (2-D analysis). Our study is based on a three-dimensional (3-D) analysis of the outcrop, including outcrops not previously described in the literature (Figure 2), and the construction, description, and interpretation of a detailed photomosaic of the coastal outcrop (Figures 3, 4). The detailed photomosaic, combined with a new set of paleocurrent data (Figure 5) and measured stratigraphic sections (Figure 6), has allowed us to determine the 3-D lithofacies distribution of the turbidite system at San Clemente.

We propose that the turbidite system at San Clemente State Beach represents the fill of a single channel cut into a low-gradient slope (see the summary interpretation at the base of Figure 4). The channel had a minimum width of about 1 km and a paleotransport direction toward the northwest (Figure 7).

PREVIOUS WORK

Weser (1971) used vertical-sequence (1-D) analysis to interpret the turbidite system at San Clemente as the fill of a channel in the proximal part of a deep-water submarine fan (the upper fan of Normark [1970]). Weser (1971) proposed that the submarine fan developed during the late Miocene in a northeast-southwest–trending embayment located south of the Los Angeles Basin. Weser (1971) inferred that the sediment source for the submarine fan was located in the present-day offshore toward the northwest. Weser's (1971) study concentrated on the south and central parts of the coastal outcrop (sections A, B, and C of Figure 2).

Walker (1975) studied the 2-D architecture of the outcrops at San Clemente State Beach, concentrating on the outcrops south of the state beach parking lot (sections A and B of Figure 2). On the basis of the lateral facies distribution, the presence of mudstone-siltstone drapes, vertical trends, and paleocurrent data, Walker (1975) suggested that the turbidite system at San Clemente represents the fill of eight nested, laterally migrating channels within the suprafan area of a submarine fan (see Walker's [1975] interpretation at the base of Figure 4). Walker (1975)

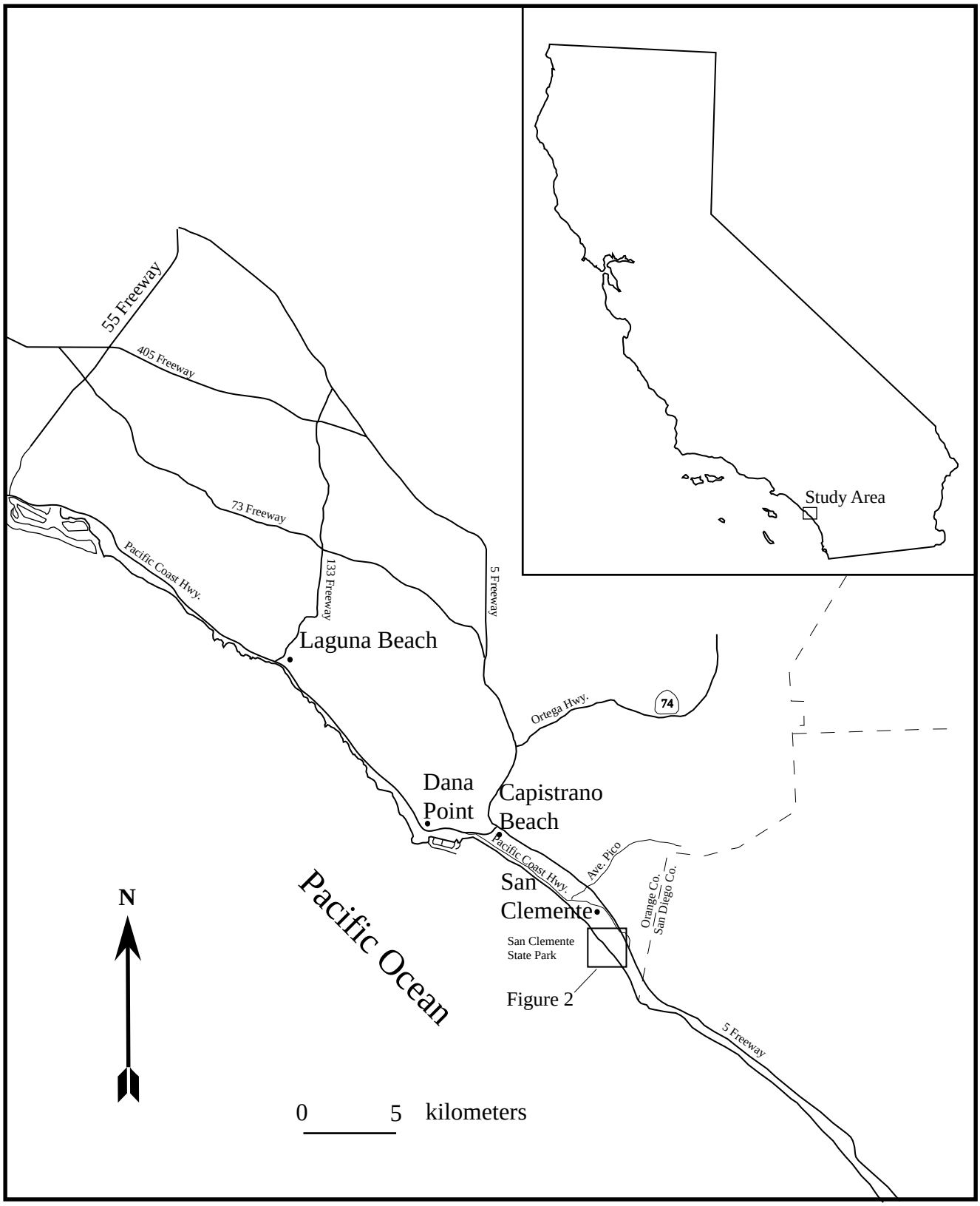

Figure 1. Location of San Clemente State Beach, showing area mapped in Figure 2.

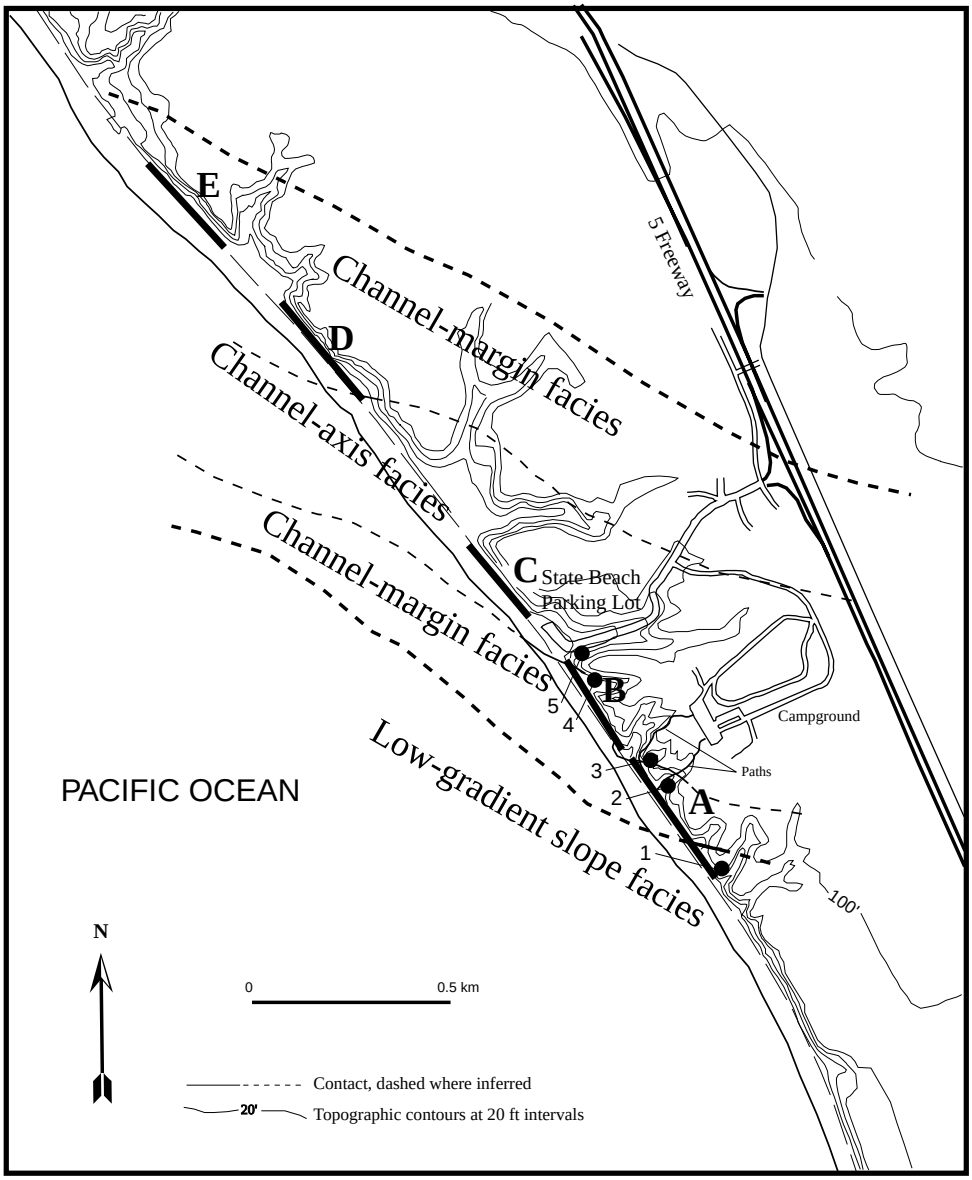

Figure 2. Lithofacies map of the San Clemente State Beach area, interpreted here as a northwest-trending turbidite channel cut into a low-gradient continental slope. Coarse-grained deposits in the center of the channel are mapped as channel-axis facies, and finer grained channel-fill deposits on either side are mapped as channel-margin facies. Very fine grained, nonslumped deposits in exposures south of the channel wall are mapped as low-gradient slope deposits. Solid lines labeled A–E show the location of photomosaics and line drawings in Figures 3 and 4. Previously published descriptions include sections A–C by Weser (1971), Hess (1979), and Clark and Pickering (1996) and sections A and B by Walker (1975). There are no previously published descriptions of sections D and E. Dots labeled 1–5 indicate locations of measured sections in Figure 6.

inferred paleotransport directions that ranged from northwest to southwest (approximately outward from the cliffs) during channel migration.

Hess (1979) expanded Walker's (1975) work by incorporating the section north of the state beach parking lot into his study (section C in Figures 2, 4). Hess (1979) agreed with Walker's (1975) interpretation of laterally migrating channels but interpreted the channel complex to have formed in a more proximal setting on an inner suprafan.

Clark and Pickering (1996) applied architectural-element analysis to the turbidite system at San Clemente, analogous to that developed for fluvial systems by Miall (1985), and concurred with Walker (1975) that the turbidite system at San Clemente State Beach represents a series of laterally migrating channels in the middle-fan area of a submarine fan.

We previously proposed that the turbidite system at San Clemente State Beach represents the fill of a single channel cut into a low-gradient slope (Busby et al., 1998; Camacho et al., 2000), and we presented our photomosaic interpretation in an informal guidebook (Nilsen et al., 2000). We formally publish our results for the first time here.

OUTCROP DESCRIPTION

We have constructed a detailed photomosaic of the sea cliffs and combined it with the mapping of side can-

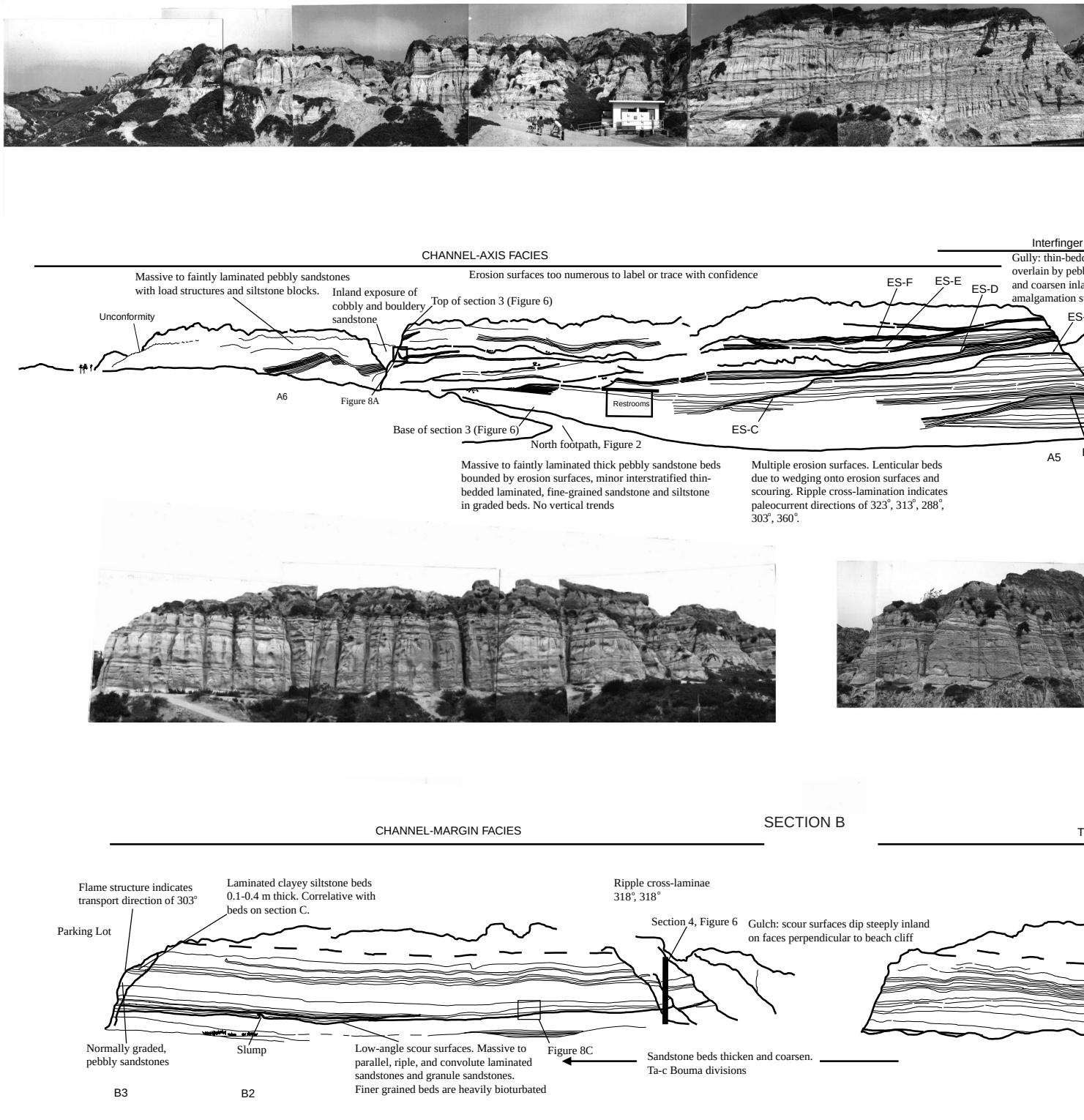

Figure 3 Southern half of the turbidite system at San Clemente (northern half shown in Figure 4). Photomosaic and line drawing of sea cliffs for sections A and B (locations shown in Figure 2). For summary interpretation, see Figure 4.

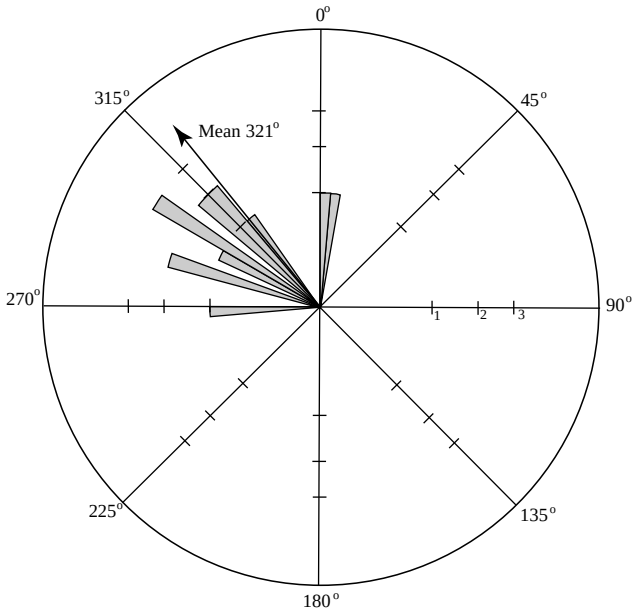

Figure 5. Paleocurrent data from channel-axis facies, channel-margin facies, and slope deposits, based on ripple cross-laminations (locations shown in Figure 3). Mean transport direction is 321° for channel deposits. This value is in agreement with measurements of the orientation of the south channel wall (plotted on Figure 3). This is also similar to the transport direction inferred from ripple cross-lamination in the low-gradient slope facies, into which the channel cuts (also plotted on Figure 3). The radius of the diagram is proportional to the square root of the frequency. Circular variance $\sigma_o = 0.1$.

yons, measurement of sections, and analysis of paleocurrent data to determine the 3-D architecture of the turbidite system at San Clemente State Beach. We divide the photomosaic into sections A–E (Figures 2, 3, 4).

Section A

Section A is the southernmost outcrop shown in the photomosaic (Figure 2). Its southern end lies approximately 600 m southeast of the state beach parking lot (Figure 2) at location A1 in Figure 3. The sedimentary rocks at location A1 are composed of massive to very thin bedded laminated mudstone and siltstone and minor sandstone. The siltstones are fine to very fine grained, with minor sandy siltstone. The massive intervals of mudstone and siltstone are heavily bioturbated. The laminated intervals reflect a lack of bioturbation and, in some cases, display slightly coarser grain size than the bioturbated intervals. The monotony of these deposits is interrupted only by the presence of five distinct, flat-lying sandstone beds at 0.5, 2.5, 3.3, 4.6, and 6.2 m above the base of the outcrop (column 1 in Figure 6). These beds are composed of white to light-gray, fine- to medium-grained sandstone. Some of the beds have planar and trough cross-lamination, representing Bouma Tb–c divisions. Cross-laminations in several of the sandstone beds indicate paleocurrent directions of 298°, 313°, 303°, 268°, and 288°. The upper three sandstone beds, which are the thickest, locally show soft-sediment deformation structures that are confined to the interior of each of these beds, each of which has planar upper and lower boundaries (Figure 3). There are no slump folds or slide scars within the siltstone section, which is flat bedded. Several samples were collected from this part of the section for micropaleontological analysis, but all were barren. The fine-grained deposits at locality A1 can be followed southward beyond the area covered by the photomosaic for more than 500 m, with no change in lithology or sedimentary structures.

The fine-grained deposits at the southernmost end of section A are cut by a prominent erosion surface (labeled ES-A) at location A2 in Figure 3, approximately 10 m northwest of location A1. The erosion surface strikes between N74°W and N64°W and dips 21°N. The sedimentary rocks that onlap the erosion surface are composed of medium- to thin-bedded, medium- to fine-grained sandstones and siltstones. The fill of ES-A contains numerous, small-scale, low-angle erosion surfaces. There is no evidence of any vertical trend in grain size or bed thickness within the fill of ES-A (Figure 3).

The fill of ES-A is in turn cut to the northwest by another prominent erosion surface, labeled ES-B (location A3 on Figure 3). Exposures do not permit us to determine whether ES-B extends to ES-B′ at locality A4 (Figure 3) or whether it lies deeper, making ES-B′ a higher erosion surface. In either case, the following relationships are observed between ES-B/ES-B′ and overlying bedding: (1) the fill is coarsest and most thickly bedded above the lowest part of the erosion surface; (2) bedding is concordant with the lowest part of the erosion surface, where it is apparently flat lying; (3) higher on the erosion surface, where that surface is steepest, it is onlapped by sandstone and siltstone that is finer grained and thinner bedded than beds lower on the surface; and (4) the highest part of the erosion surface is draped by the finest grained and thinnest beds in the section. This lateral change is accomplished by abrupt thinning and fining of individual beds onto the erosion surface. There are, however, no vertical trends in bed thickness or grain size within the fill of ES-B.

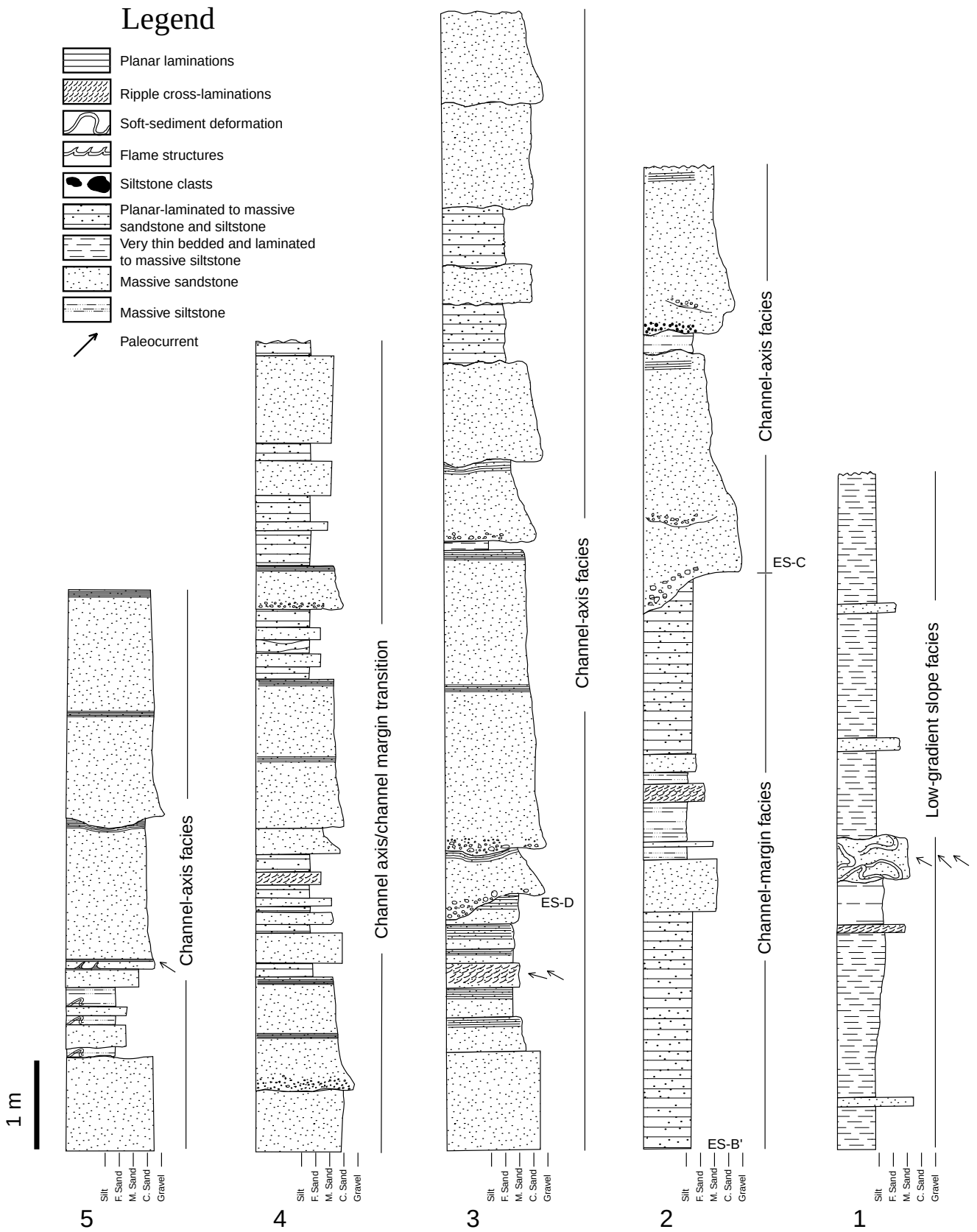
Legend
Planar laminations
Ripple cross-laminations
Soft-sediment deformation
Flame structures
Siltstone clasts
Planar-laminated to massive sandstone and siltstone
Very thin bedded and laminated to massive siltstone
Massive sandstone
Massive siltstone
Paleocurrent
1 m
Channel-axis facies
Channel axis/channel margin transition
Channel-axis facies
ES-D
Channel-axis facies
ES-C
Channel-margin facies
ES-B'
Low-gradient slope facies
Silt
F. Sand
M. Sand
C. Sand
Gravel
5
4
3
2
1

Figure 6. Representative measured sections through low-gradient slope facies, channel-margin facies, and channel-axis facies of the San Clemente turbidite system. The low-gradient slope facies consists of very thin bedded, planar-laminated to massive, bioturbated siltstone, with minor ripple cross-laminated, fine-grained to medium-grained sandstone with local soft-sediment deformation structures. The channel-margin facies consists of thin-bedded to medium-bedded, planar-laminated, ripple cross-laminated and massive, silty medium-grained sandstones and lesser thick bedded, massive, medium-grained to coarse-grained sandstones. The channel-axis facies consists of very thick bedded, normally graded, coarse-grained sandstones and lesser pebble conglomerates, with Bouma A and B divisions, and abundant basal scours and amalgamation surfaces. Although there are many graded beds, we recognize no vertical trends through multiple beds, such as fining- or thinning-upward sequences of beds; nor do we recognize thickening- or thinning-upward sequences of beds. ES-B′, ES-C, ES-D = erosion surfaces mapped on Figure 3.

The concordant, lower part of the fill of ES-B is shown in the lower half of measured section 2, below erosion surface C (ES-C) (Figure 6). This part of the section consists of thin-bedded, fine-grained to medium-grained, massive sandstone and siltstone interbeds and minor thick-bedded, medium-grained sandstone. The thick beds clearly thin and fine laterally toward ES-B and merge into the very thin bedded drapes high on the erosion surface. We refer to the very thin bedded drapes high on the erosion surface as sandstone-siltstone couplets, because they consist of alternating very thin beds of fine-grained sandstone and siltstone. Measurements taken on ES-B′ show it has a strike of N87°W and dips 22°N (Figure 3).

Erosion surface C appears to be nearly horizontal along the cliff face south of the southern footpath, but it steepens and cuts downsection on the cliff face north of the footpath (Figure 3). However, the steepest apparent dips on ES-C are in the side canyon that contains the southern footpath (Figure 3), where it dips

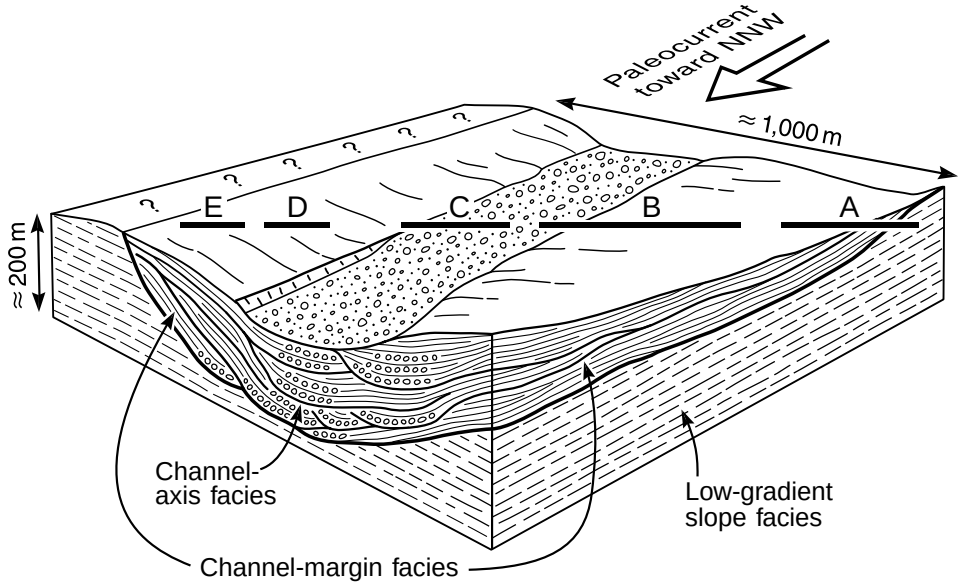

Figure 7. Schematic depositional model for the turbidite system at San Clemente State Beach, based on the photomosaic and line-drawing interpretations of Figures 3 and 4. A single turbidite channel was cut into fine-grained sediments deposited on a low-gradient continental slope and filled by vertical aggradation. The low-gradient slope deposits at the present-day level of exposure were all deposited before the turbidite channel was cut. We interpret multiple erosion surfaces within the turbidite channel to record lateral shifting of the channel thalweg (not separate turbidite channels) with time. Lateral shifting of the thalweg resulted in interfingering of channel-axis and channel-margin deposits. Heavy lines labeled A–E show approximate locations of photomosaics and line drawings presented in Figures 3 and 4, and a single, simplified section of the system is drawn to scale, with no vertical exaggeration, at the bottom of Figure 4. Question marks shown outside the turbidite channel refer to the fact that any sediment that presumably existed above the present-day cliff tops is not preserved. Therefore, we cannot determine whether (1) coeval sedimentation outside the turbidite channel was dominated by overbanking and building of sandy levees or (2) the channel was deep enough (and/or turbidity currents dense enough) to prevent overbanking, resulting in ongoing low-gradient slope mud sedimentation outside the turbidite channel (see Figure 9).

steeply inland (to the east-northeast). The fill of ES-C in the side canyon forms the upper half of measured section 2 (Figure 6) and is thick-bedded, coarse- to medium-grained sandstone and conglomerate in highly erosively based beds, with numerous amalgamation surfaces and load structures. Normal grading is common, with planar or convolute lamination at the tops of beds. Many of the beds have basal shale clast concentrations. On the cliff face near locality A3 (Figure 3), ES-C approaches ES-B and becomes parallel with it, and the beds above ES-C thin toward ES-C and drape it (Figure 3).

Erosion surfaces become so numerous north of the southern footpath (locality A5 in Figure 3) that it is difficult to correlate them across the side canyon (see ES-B′ and ES-C in Figure 3). These are in turn overlain by very closely spaced erosion surfaces (ES-D, ES-E, ES-F). Erosion surfaces then become so closely spaced that we do not attempt to label them individually between localities A5 and the northern end of section A (Figure 3). In fact, many beds are bounded both below and above by erosion surfaces. These erosion surfaces show maximum dips in exposures perpendicular to the cliff face. A representative section (column 3 in Figure 6) was measured along the northern footpath (Figure 3). The fill of ES-D, ES-E, ES-F, and so on consists largely of very thick bedded and lesser medium-bedded, medium-grained to coarse-grained sandstone and conglomerate, in graded beds that are largely massive, with planar laminations near the tops of some beds. This coarse-grained lithofacies includes isolated load balls of cobble conglomerate. Exposures along the northern footpath also include an example of a so-called flap of siltstone arrested in the process of being ripped up (Figure 8A). The very thick beds in the measured section of the northern footpath (column 3 in Figure 6) form part of a coarse-grained lithofacies belt that can be mapped behind the cliffs directly into thick beds in the measured section of the southern footpath (column 2 in Figure 6), as shown by the facies map of Figure 2. Based on our mapping of erosion surfaces, however, the beds in column 3 in Figure 6 must be younger than most of the beds in column 2.

Section B

An erosion gap in the cliffs lies between sections A and B, as shown to scale in our interpretive summary at the base of Figure 4. At the southern end of section B (locality B1) is a thick (1.5 m), massive, pebbly sandstone bed full of shale clasts ranging in size from a few centimeters to greater than 1 m (Figure 8B). The rip-up clasts maintain their internal structure, showing little deformation. The composition and internal sedimentary structures of the clasts are very similar to the sandstone-siltstone couplets described in section A (Figures 3, 4). The base of the bed is eroded into a thin-bedded sandstone-siltstone couplet section that may be correlative with the disrupted, thin-bedded section at locality A6. The pebbly sandstone bed with shale clasts is overlain by a series of two graded, cobble- to pebble-sandstone beds, 1–2 m thick. The upper of the two beds is cut by an erosion surface (ES-G) that was filled by thin-bedded sandstone-siltstone couplets and was in turn cut by the erosion surface labeled ES-H. This surface is filled with a thick, massive sandstone that was in turn eroded along ES-I (Figure 3). That surface is in turn overlain and onlapped by a very thick bed and overlying medium beds of massive, coarse-grained sandstone. These in turn are cut by ES-J, a low-angle scour draped by thin-bedded sandstone-siltstone couplets. This erosion surface is one of many low-angle erosion surfaces that progressively steepen northward between ES-J and ES-K (Figure 3). The flatter segments of erosion surfaces are draped by sandstone-siltstone couplets, whereas the steeper segments of erosion surfaces are onlapped by the sandstone-siltstone couplets.

Erosion surface K (ES-K in Figure 3) marks the beginning of a section, extending to the end of section B (locality B3), where erosion surfaces are not obvious along the cliff face. They are obvious, however, in exposures perpendicular to the cliff face. Erosion surface K is onlapped and draped by sandstone-siltstone couplets similar to those below ES-K, but they pass laterally (northward) into thick-bedded to very thick bedded sandstones that extend to the northern end of section B (Figure 3). These thick-bedded to very thick bedded sandstones occur in intervals that alternate with intervals of medium-bedded, muddy siltstones and fine-grained sandstones (column 4 in Figure 6). The very thick bedded to thick-bedded sandstones are commonly massive, but some either contain Bouma Ta–c divisions (Figure 8C) or are planar laminated. The medium-bedded, muddy siltstones and fine-grained sandstones are dominated by Bouma Tb–c divisions. Sedimentary structures include load structures, dish structures, and burrows that are commonly bedding parallel, although some cross the beds. Siltstone clasts include gray mudstone in some beds and

black carbonaceous mudstone in other beds. A soft-sediment slump involving several beds is present at locality B2 (Figure 3). This slumped horizon is also locally present but thicker behind the cliffs at the northern end of section B (column 5 in Figure 6). This measured section shows that sandstones thicken and coarsen very rapidly behind the cliff. A flame structure in column 5 in Figure 6 suggests a paleocurrent direction of 303°.

Section C

Exposures between section B and section C are semicontinuous around the state beach parking lot, and the medium-bedded section at the base of the cliff at locality C1 (Figure 4) appears to be correlative with the medium-bedded section on the south side of the parking lot at locality B3 (Figure 3). The upper part of the cliff at locality C1, however, contains coarse-grained sandstones, pebbly sandstones, and conglomerates in very thick, amalgamated beds; these are not present on the south side of the state beach parking lot. The coarse-grained, very thick bedded strata lie above a pronounced erosion surface (ES-L in Figure 4), and they dominate section C.

The bedding in section C is characterized by curved, nonparallel, and, in some cases, lenticular beds (Figure 4). There are abundant erosion and amalgamation surfaces. The apparent dips of the erosion surfaces are both to the south and north; however, south-dipping erosion surfaces become more dominant toward the northern end of section C (Figures 4, 8D). Erosion surfaces are commonly lined with pebble stringers (Figure 8D) or with siltstone clasts (Figure 8E, F). The sandstone-conglomerate beds are commonly massive, and most are normally graded, although some contain pebbles evenly dispersed throughout the bed (locality C2 in Figure 4). Discontinuous pebble trains locally define a crude lamination within some beds (e.g., localities C3 and C4 in Figure 4). The sandstone-conglomerate beds show load structures where they overlie medium-bedded, fine-grained sandstones and siltstones (Figure 8E, F). Excellent exposures, perpendicular to the cliff face, are present in the side canyon at the northern end of section C, and the deepest scours occur there.

Within the normally graded sands and gravels of the channel-axis facies of section C (as well as section B) are areas or entire beds of sandstone or pebbly sandstone containing subrounded to angular clasts of siltstone, ranging in size from a few centimeters to rafts more than a meter in length (Figure 8B). These may constitute discrete beds or lenses of matrix-supported siltstone-clast conglomerate or form gradationally bounded patches rich in siltstone clasts within otherwise structureless or normally graded sandstone or pebbly sandstone. The siltstone within the clasts is similar to siltstones in the local sequence.

The biggest gap in our photomosaic (300 m) lies north of section C, where the outcrop is covered by vegetation and has been degraded by the real estate development of the area. There is no outcrop at all for the southern third of this distance, and the northern two-thirds has sporadic, poor outcrop along the small gully shown in Figure 2. These outcrops consist of medium- to thick-bedded, fine- to medium-grained sandstones. Beachward of these sandstones is a very poorly exposed section of mudstones and siltstones that is unlikely to be in place, because basketball courts, fences, and concrete walls are slipping down this slope.

Section D

The southernmost end of section D (locality D1 in Figure 4) contains the only thin- to medium-bedded siltstones and sandstones in section D. These are interstratified with very thick bedded, pebbly sandstones (locality D1). This sequence is cut by a prominent, deep erosion surface (ES-M in Figure 4). The erosion surface is onlapped by at least one bed, which thins toward the onlap, and this bed is in turn apparently downlapped by three more beds. The top of these three beds has been partly removed by ES-N, which appears to merge southward with ES-M (Figure 4). The cliff face from locality D1 to locality D2 has numerous water seeps that result in growth of algae and moss, so sedimentary textures and structures are very poorly displayed. Fresh rockfall fragments at the base of the cliff show that the sands are planar laminated, with uncommon cross-laminations. Bedding between localities D1 and D2 is relatively parallel and continuous. The rest of section D to the north of locality D2, in contrast, has extremely lenticular bedding. The section of lenticular beds lies above an erosion surface at the northern end of the outcrop (ES-O in Figure 4). The lenticular beds are dominantly massive, with local planar or convolute laminations, and are very thick, amalgamated beds with basal scours. Siltstone clasts up to 0.5 m are more abundant here than anywhere else at San Clemente (Figure 4). These clasts are both dispersed through the beds and

A

B

Figure 8. Outcrop features of the San Clemente turbidite system. The positions of these photographs are plotted on Figures 3 and 4. (A) Incorporation of siltstone substrate into the base of a high-density turbidity current, apparently frozen into place before any downstream transport occurred (channel-axis facies in section A in Figure 3) (B) Large siltstone clasts within massive, pebbly sandstone of the channel-axis facies (section B in Figure 3). This bed is overlain by two normally graded conglomerate to sandstone beds (bases marked by arrows). Continued.

concentrated above basal scours. The beds below the erosion surface at the northern end of section D (ES-O) are not well exposed in the sea cliff but are well exposed inland, where they consist of medium- to thick-bedded, fine- to medium-grained sandstones. These beds are also discontinuously exposed in the 150 m gap between section E and section F, which is largely covered by houses.

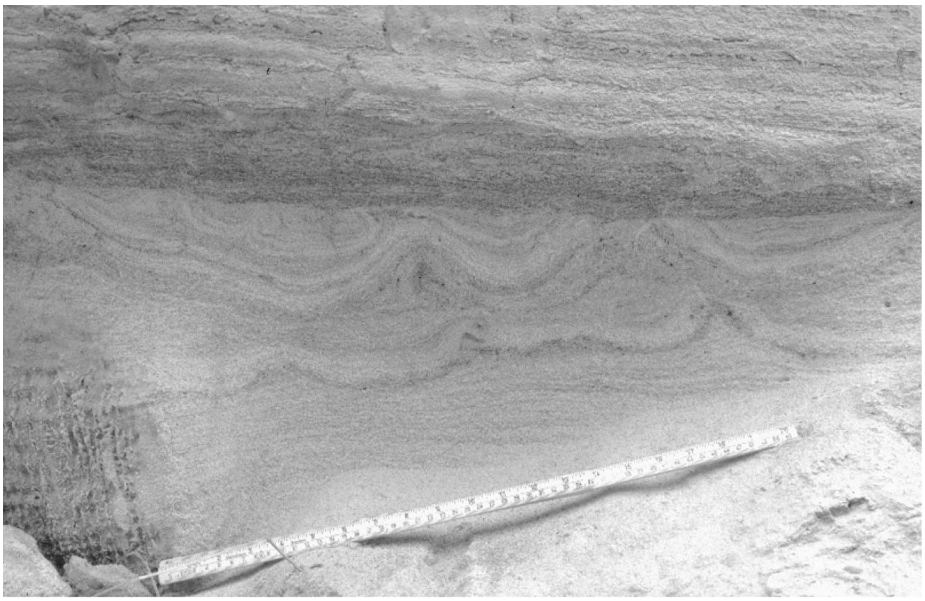

C

D

Figure 8. Continued. (C) Bouma Tb and Tc divisions in thick-bedded sandstone, overlain by laminated silty sandstone; from the channel-margin facies near the northern end of section B (Figure 3). Yardstick for scale. (D) Coarse-grained sandstone and pebble to cobble conglomerate of the channel-axis facies (section C in Figure 4). Sandstones and conglomerates are stratified to massive and commonly normally graded. Scour surfaces are numerous (some pointed out by arrows). Fine-grained sandstones and siltstones are uncommon, except as intraclasts. Continued.

Section E

The northern third of the outcrop shown in section E (Figure 4) is presently covered by a slide that formed during the El Niño storms of 1998, after we shot our photomosaic. Section E is composed of thin- to medium-bedded, fine- to coarse-grained sandstone, siltstone, and clayey siltstone. This section is very similar to the part of section A between localities A3 and A5 and to the part of section B between ES-J and ES-K. As in these sections, numerous low-angle erosion surfaces are present, but in section E, these dip southwestward, in contrast to the northward dip of erosion surfaces in sections A and B.

LITHOFACIES DISTRIBUTION AND PALEOCURRENT DATA

We recognize three main lithofacies, interpreted to represent slope, channel-margin, and channel-axis deposits, based on our 3-D facies analysis. The prechannel,

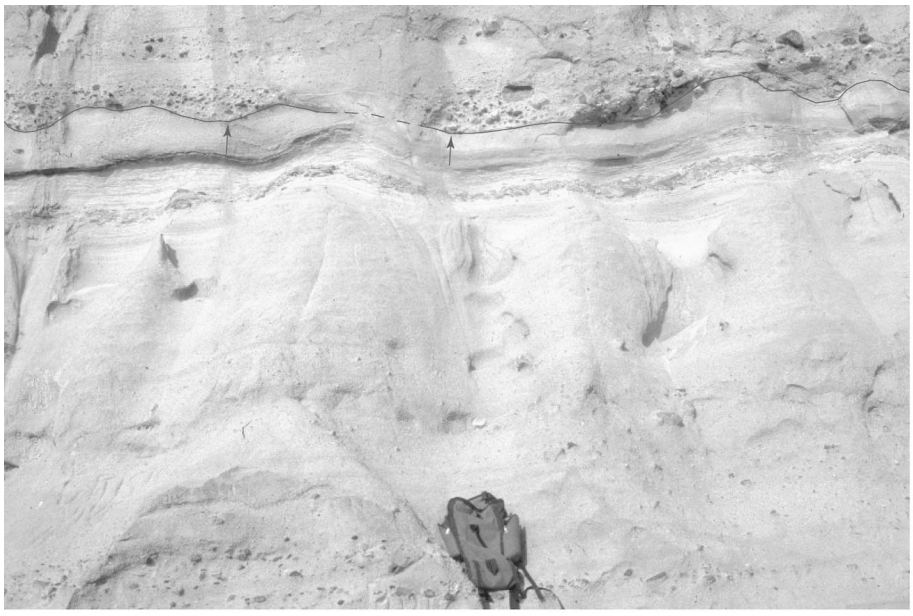

E

F

Figure 8. Continued. Close-up (E) and detailed (F) views a of channel-axis facies, showing uncommon occurrence of interstratified fine-grained sandstone and siltstone (section C in Figure 4). Pebbles and cobbles are commonly confined to the floors of scours (e.g., above the vertical arrows in E), although some occur as layers within beds (e.g., along the horizontal layers). Continuous layers of siltstone intraclasts (e.g., marked with a solid line below it) probably formed by disruption of siltstone beds by turbulent flows. The object in E is approximately 58 cm tall.

low-gradient slope facies occurs in the southernmost part of section A (Figure 3). The channel-margin facies occurs in parts of sections A, B, D, and E (Figures 3, 4). The channel-axis facies occupies all of section C and also parts of sections A and B (Figures 3, 4). We show here that the lithofacies distribution (Figure 2), together with the paleocurrent data (Figure 5), indicate that the turbidite channel has a southeast-northwest trend, with a paleotransport direction toward the northwest.

Low-Gradient Slope Deposits (Prechannel)

We concur with Weser (1971) that the siltstones and mudstones that extend at least 500 m southward from the southern end of section A (Figure 3) represent slope deposits, but we infer them to represent low-gradient slope deposits rather than the deposits typical of high-gradient continental slopes. The slope section lacks soft-sediment deformation structures, such as slump-folded sections, slide scars, or slide blocks, sug-

gesting that a low-gradient, rather than a high-gradient, continental slope is represented. Only the three thickest sandstone beds show any soft-sediment deformation, and that deformation is internal to each bed (Figures 3, 6). These probably formed by liquefaction penecontemporaneous with deposition and do not record wholesale slumping of a section. Significant slump folding appears to occur on continental slopes with gradients greater than 1°. For example, Kenyon et al. (1978) reported abundant slump folds on slopes between 3 and 5° in the Bay of Biscay (northern Spain), and Lewis (1971) reported slumps on slopes between 1 and 4° off Hawkes Bay Land District in New Zealand.

The slope deposits were deposited below wave base, because they show no evidence of wave-generated sedimentary structures and they have a major turbidite channel cut into them, supporting the interpretation that they are deep-water deposits. Paleobathymetric data are not available from San Clemente State Beach, unfortunately, because our samples are barren, possibly due to dissolution in the outcrop. The same lithofacies in the Capistrano Formation at Dana Point (Figure 1), however, has yielded benthic foraminifera assemblages that indicate deposition at bathyal water depths (Ingle, 1971).

At the current level of erosion, it is not possible to completely discard the possibility that the San Clemente channel was leveed, because no time-equivalent sediments are preserved above the modern sea cliffs outside the turbidite paleochannel and probably only a small part of the entire thickness of channel fill is preserved. The fine-grained deposits at the southern end of section A (Figure 3) predate the channel, which is cut into them. We interpret these to be slope deposits, rather than levee deposits, for two reasons. First, one of the key diagnostic features of levee deposits is the presence of slumps directed away from the channel (Morris and Busby-Spera, 1990). All types of channels may have slumps directed inward toward the channel axis, because bank undercutting is common; levees, however, have positive depositional relief above the rest of the fan surface (or basin floor surface), so they also collapse outward (e.g., Kenyon et al., 1995). Slump folds and slide scars are absent from the slope deposits of the San Clemente section. Second, modern and ancient levee deposits show paleocurrents directed at some angle away from the main channel axis. Hiscott et al. (1997a, p. 76) estimated paleoflow directions of overspill deposits in the levees of the Amazon Fan channel, based on the anisotropy of magnetic susceptibility of elongated silt-size to sand-size particles, and concluded that paleoflow directions are "broadly away from the main channel axis" but with considerable dispersion, partly because of topographic complexities and partly because of overspill from neighboring channel bends. Our data, in contrast, show low dispersion ($\sigma_o = 0.1$) and are parallel to paleocurrent measurements from deposits within the channel. We conclude that the fine-grained section represents slope, rather than levee, deposits.

Another possibility is that the fine-grained deposits at the southern end of section A (Figure 3) represent basin-floor deposits, but we would not expect the turbidite channel that is cut into these deposits to contain cobbles in its fill if it had a nearly horizontal axial gradient. Turbidite channels can carry sand on basin floors with gradients of 0.2° (Carter and Carter, 1996), but we are not aware of any basin-floor turbidite channels with cobbles in their fill. Finally, one could argue that the fine-grained deposits are significantly older than the turbidite channel that is cut into them and, therefore, could have formed in a completely different depositional environment than that of the turbidite channel. However, the fine-grained section appears to have been unlithified when the turbidite channel was cut into it, as shown by small-scale irregularities along the erosion contact, as well as the absence of sandstone blocks in the channel fill (criteria used by Morris and Busby-Spera [1988]).

In summary, we conclude that the fine-grained deposits at the southern end of San Clemente State Beach accumulated on a low-gradient slope that was too gentle to produce slumps but steep enough for turbidity currents to transport gravel.

Channel-Margin Deposits

We interpret the erosion surface at the southern end of section A (ES-A, location A2 in Figure 3) to represent the southern wall of a single turbidite channel whose fill extends to the northern end of the section described in this article (section E in Figure 4). There is a very marked contrast in lithology across the turbidite channel wall, with siltstone below and sandstone above, and numerous sandstone beds onlapping the channel wall. All of the other erosion surfaces in the section are closely spaced surfaces that have similar rock types below and above them (dominantly sandstone) and are filled with one to several beds that thin and drape onto the erosion surface. We interpret these to record localized, temporary episodes of scouring by relatively erosive turbidity currents within a much

larger turbidite channel that was overall aggradational in character. We do not interpret them to be channel walls. Our usage of "scours" vs. "channels" follows the widely accepted definition of channel as a "long-term pathway for sediment transport" (Mutti and Normark, 1987, p. 9).

The channel-margin facies is recognized as fine- to medium-grained, thin- to medium-bedded siltstones and sandstones, with erosion surfaces dipping northwest in the southern channel-margin deposits (sections A and B in Figure 3) and erosion surfaces dipping southwest in the northern channel-margin deposits (sections D and E in Figure 4). The northern channel wall is not exposed, so we can only provide a minimum estimate of channel width (1 km). If the abundant, large siltstone clasts in the northern part of the channel-margin facies (section E in Figure 4) were derived by bank collapse of the northern channel wall, however, it probably did not lie far away, and our minimum estimate is close to the true channel width.

Channel-Axis Facies

The channel-axis facies is distinguished by its coarse grain size (coarse sand to cobbles), very thick bedding, amalgamation surfaces, lack of siltstone interbeds, and the subhorizontal and symmetrical geometry of erosion surfaces (section C in Figure 4; Figure 8D, E).

The channel-axis facies gradationally interfingers with the channel-margin facies over lateral distances of 100 m or less (sections A, B, and C in Figures 3, 4). The map-scale irregularities in the channel axis–channel margin contacts (Figure 2) are also apparent in the sea cliffs (Figures 3, 4) and probably result from minor, lateral migration of the turbidite channel thalweg as the channel aggraded.

Paleocurrent Data

Paleocurrent directions from intrachannel deposits, as well as prechannel slope deposits, are all approximately the same (Figure 5). Our paleocurrent measurements ($n = 14$), taken from ripple cross-lamination and one flame structure, range from 270 to 3°. For channel deposits, the average transport direction is 321°, and where both the channel sediments and slope deposits are considered, the average transport direction is 311°. This average transport direction is in agreement with our measurements of the orientation of the southern channel wall (286 and 296°). Walker (1975) and Hess (1979) obtained paleocurrent directions similar to ours from ripple cross-laminations from prechannel and channel-fill rocks. However, most of Walker's (1975) paleocurrent measurements used apparent dips of erosion surfaces on the cliff face, which actually dip into the cliff face; these yielded paleocurrent directions that are perpendicular to our measurements.

Discussion

We see no vertical trends, in terms of bed thickness or grain size, on our photomosaic line drawings (Figures 3, 4) or on our measured sections (Figure 6). We do not recognize the thickening- and coarsening-upward sequences of beds reported by Walker (1975) and Hess (1979) and interpreted to represent lobe progradation. Nor do we recognize the thinning- and fining-upward sequences of beds that they inferred to record channel-abandonment cycles (Walker, 1975; Hess, 1979). Thinner/finer and thicker/coarser beds alternate without any vertical pattern, although rapid lateral changes occur between the channel-margin facies and the channel-axis facies.

Walker (1975) interpreted the section to represent a series of eight laterally migrating channels, separated by what he termed "siltstone-mudstone drapes" (see Walker's [1975] lateral section and interpretation, reproduced at the base of Figure 4). We do not recognize siltstone-mudstone drapes, although we do recognize sandstone-siltstone couplets that thin toward and onlap or drape some of the erosion surfaces (in the channel-margin facies in Figures 3, 4). We suggest that the sandstone-siltstone couplets represent deposition from the low-density part of the turbidity currents at higher levels within the main channel (channel margin) at the same time that the high-density (basal) part of the turbidity currents moved through lower parts of the channel (channel-axis facies; see the following process sedimentology section). The scours lined by sandstone-siltstone couplets are not channels; instead, they are scours within the main channel, and they were cut by more energetic flows that locally passed down the channel.

The only sizable gap in good exposure through the San Clemente turbidite system lies between sections C and D, as described previously. If our interpretation is correct and the poorly exposed mudstones along the beach represent modern slumps covering sandstones that sporadically outcrop in the small inland gully (Figure 2), then gap 3 (summary interpretation in Figure 4) can be mapped as part of the channel axis–channel margin transition. Alternatively, if the mudstones and

siltstones along the beach at gap 3 are not modern slide deposits, then these deposits may represent (1) a mud plug developed in the turbidite channel during a period of abandonment, (2) a slide sheet or block deposited within the turbidite channel, or (3) interchannel deposits, between two adjacent channels represented by sections D and E and by sections A, B, and C, respectively. We, however, believe that the sandstones exposed in the gully behind the sea cliff are in place and that the mudstones and siltstones in gap 3 (Figure 4) are the result of pronounced landslide activity along San Clemente sea cliffs (Abbott, 1999).

PROCESS SEDIMENTOLOGY

We concur with Walker's (1975) suggestion that the lateral equivalence of drapes high on the erosion surfaces, with thicker sands lower on these surfaces, is a result of flow stratification. Sand was mainly transported low in the flows and was more confined toward the bathymetrically lower channel axis, whereas silt was carried in more uniform suspension. We see no reason to invoke different explanations, such as temporary channel abandonment (Walker, 1975), as an explanation for drapes; the surfaces that appear to be draped throughout the height of the present-day outcrop likely pass below outcrop level into thick sands, just as many others do within the outcrop.

Significant surfaces of erosion within the channel-margin facies are commonly separated by more beds than they are in the channel-axis facies, indicating that erosion higher on the channel sides was a comparatively infrequent occurrence. Within the channel axis, in contrast, all of the larger flows (or at least those that left a depositional record) were initially erosional, because virtually all thick beds in the channel-axis facies have significant erosion surfaces at their bases. The presence of pebbles and cobbles confined to the floors of scours and of isolated load balls of conglomerate indicates that there was considerable bypassing of gravelly material down the axial part of the channel during initial (erosional or nondepositional) stages of flow. Most of these coarse-grained deposits show normal grading, suggesting that the initiation of deposition from each flow in the channel axis was triggered by waning of the current, which then infilled scours created by the same current during its earlier stages.

Siltstone clast–rich beds are restricted to the channel axis (see the preceding description of section C), which indicates that the flows (or parts of flows) from which they were deposited were very dense. It seems unlikely that rafts of silt could be transported significant distances by rolling or sliding along the bed. This implies that the transport mechanism involved support by frictional strength of the sandy matrix. However, the mechanical properties of such high-concentration sandy dispersions argue against sandy debris flow as a long-distance transport mechanism on low slopes (e.g., Hiscott et al., 1997b; Kneller and Buckee, 2000). We interpret these deposits as a result of a transient transport/depositional regime involving a high-density, mobile layer of sand at the lower flow boundary (a so-called quick bed), possibly undergoing laminar flow, and supported by dispersive pressure and upward displacement of water (Kneller and Branney, 1995). Such high-concentration layers may develop at the base of strongly depositional currents (Middleton, 1967; Vrolijk and Southard, 1997). They are supplied by sediment that falls out of suspension from the overlying current, and they in turn supply sediment to the bed by progressive freezing at the base. They are driven by the residual momentum of sediment that enters from above and by shear from the overriding flow. We suggest that these layers may locally cut down into the substrate by injection or plowing (Branney et al., 1990), incorporating rafts of silt and transporting them a short distance downstream before part of the layer carrying the silt clasts freezes due to frictional forces. The incorporation of silt substrate is locally recorded by freezing of the layer during the process of injection (Figure 8A) before any downstream transport has occurred.

We do not consider the siltstone clast–rich sandstone beds to be the result of cohesionless or sandy debris flow (cf. Shanmugam, 1996), because, in our interpretation, the high-density layers that produced them were generated and driven by an overlying turbidity current. Sand was likely transported most of the distance from the shelf, suspended within the turbidity current; the high-density layer into which siltstone clasts were incorporated only came into existence as the flow began to collapse. This mechanism is feasible on small or even zero slopes and is consistent with the implied formation of high-density basal layers through high suspended-sediment fallout rates. The presence of massive deposits within the channel axis (indicating high sediment-load fallout rates) and weakly developed traction structures elsewhere all suggest rapidly waning flows (Kneller and McCaffrey, 1995).

At least one major phase of channel incision occurred to produce the main bounding erosion surface

(ES-A). The channel axis facies represents aggradation of the channel within a broader confining erosion surface, with the channel facies retaining their character through the vertical succession and channel confinement being maintained by deposition of fine sediment at the channel margins.

MODERN ANALOGS

We propose the Gollum channel system (Kenyon et al., 1978) on the eastern slope of the Porcupine Seabight, between western Ireland and northern Spain, as a modern analog of the turbidite system at San Clemente, California (Figure 9). The Gollum system consists of a dendritic system of channels developed on a nonslumped continental slope of low gradient (about 0.5°) (Kenyon et al., 1978). The channels show no evidence of levees. They are smaller and have flatter floors than the steep-walled submarine canyons developed on high-gradient, slumped continental slopes. The bottoms of the channels appear dark-toned on the sonographs, indicating coarser material (axial facies), suggesting that the channels are still active (Kenyon et al., 1978).

A second possible modern analog of the Miocene San Clemente turbidite system lies in the same California borderland tectonic setting only 30 km northwest of San Clemente. This is an unnamed deep-water channel system running southward down the continental slope offshore of Newport Beach, about 10 km east of the San Gabriel Submarine Canyon (Marlow et al., 2000, figures 2, 5). The lower two-thirds of this channel system lies on a low-gradient slope of approximately 1°, although the upper third of the system lies on a 3° slope, which is steeper than we envision for the San Clemente turbidite system.

The turbidite system at San Clemente may represent one single channel within a system of channels that developed during the Miocene. The Doheny

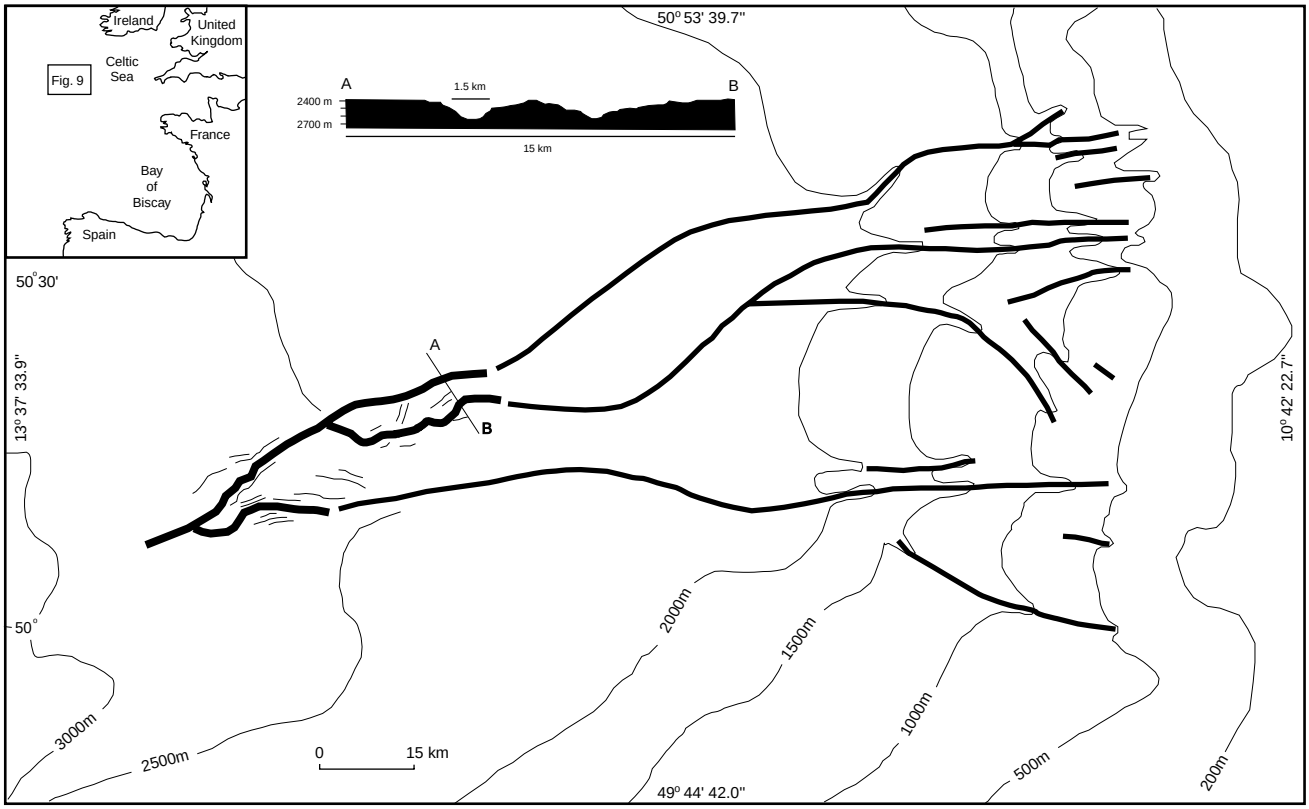

Figure 9. Proposed modern analog of the San Clemente turbidite system: the Gollum channel system of the Porcupine Seabight off southwestern Ireland (Kenyon et al., 1978). These channels are cut into a low-gradient continental slope (0.5°) that has no detectable slump structures. These low-gradient slope channels contrast markedly with the steep-walled, large, V-shaped canyons typical of slumped, high-gradient continental slopes (e.g., Bay of Biscay) (Kenyon et al., 1978). The low-gradient slope channels are smaller and shallower and have flatter floors than submarine canyons (see inset cross section). The faint lines drawn just outside the channels on this figure may represent terraces, and there is no evidence of levees on the channels (Kenyon et al., 1978).

Channel at Dana Point 10 km to the north may represent another channel in this system.

POTENTIAL APPLICATIONS TO PETROLEUM GEOLOGY

The outcrops at San Clemente have been used both as a training site and as an outcrop analog for hydrocarbon reservoirs in channelized turbidite systems (e.g., Campion et al., 2000). Outcrop relations from analogs can provide architectural detail (such as facies geometry, transitions, bed-length data, etc.) at a scale that is seismically irresolvable. Such information may be used either as input to stochastic models or in the construction of deterministic models. Their value in reducing uncertainty in the subsurface is considerably compromised where there are uncertainties in the actual geologic interpretation of the outcrops.

In the case of the San Clemente Channel, the principal controls on performance of these channelized turbidites as a potential reservoir are (1) the overall form of the sand body and (2) the form of the fine-grained drapes within it. We suggest that the thickness of the channel body is substantially greater than the small thickness of section now exposed on the shore (cf. Campion et al., 2000). Merely projecting the bounding erosion surface into the subsurface as a circular arc suggests approximately a 200 m thickness of channel fill below the current exposure level. Similarly, because the axial facies represents material deposited in deeper parts of the channel, time-equivalent channel-margin facies would lie above the present-day erosion surface. The section presently exposed represents a thin slice through an aggrading system that is largely in the subsurface or eroded and whose overall architecture must be inferred from the exposed section.

We argued in preceding sections that the fine-grained intervals formed as a consequence of flow stratification and that they pass into coarser grained, more permeable material down the dip of the erosion surfaces that they drape (i.e., toward the channel axis). Thus, the siltstone drapes merely constitute baffles inclined toward the channel axis and elongate parallel to it. We suggest that close to the channel axis, there are no significant barriers to fluid flow. Some of the fine-grained drapes appear to form continuous barriers to fluid flow, but we suggest that this is merely a function of the present level of exposure and that they, too, pass into sand-on-sand contacts in the subsurface. Flow simulations, synthetic seismograms, and geologic interpretations based solely on the present level of exposure yield a substantially different picture from that based on geologically inferred projections beyond the present outcrop.

CONCLUSIONS

The turbidite system at San Clemente State Beach represents the fill of a single turbidite channel that was cut into fine-grained sediments deposited on a low-gradient, continental slope and filled by vertical aggradation. The low-gradient slope deposits at the present-day level of exposure were all deposited before the channel was cut, and the slope was too gentle to produce slumps but steep enough for turbidity currents in the channel to transport gravel. We cannot determine whether overbank deposition built levees coeval with channel filling, because any sediment that presumably existed above the present-day cliff tops is not preserved. The transport direction in the turbidite channel was 321°, nearly parallel to the present cliffs. Coarse-grained deposits in the center of the turbidite channel are mapped as channel-axis facies, and finer grained channel-fill deposits on either side are mapped as channel-margin facies. We interpret multiple erosion surfaces within the turbidite channel to record lateral shifting with time of the channel thalweg (not separate turbidite channels). Lateral shifting of the thalweg coupled with vertical aggradation resulted in interfingering of channel-axis and channel-margin deposits.

Proposed modern analogs of the San Clemente turbidite system include the Gollum channel system of the Porcupine Seabight off southwestern Ireland (Kenyon et al., 1978) and an unnamed channel system offshore of Newport Beach in southern California (Marlow et al., 2000).

REFERENCES CITED

Abbott, P. L., 1999, Natural disasters: Boston, McGraw-Hill, 397 p.

Branney, M. J., B. Kneller, and B. P. Kokelaar, 1990, Disordered turbidite facies (DTF): a product of continuous surging density flows (abs.): International Association of Sedimentologists, Comparative Sedimentology Division, International Sedimentological Congress, v. 13, p. 38.

Busby, C. J., H. Camacho, and B. Kneller, 1998, A new model for the Miocene–Pliocene turbidite system at San Clemente, CA (abs.): AAPG Bulletin v. 82, p. 844.

Camacho, H., C. J. Busby, and B. Kneller, 2000, A 90 degree turn on the interpretation of the classical turbidite locality at San Clemente, California (abs.): AAPG Annual Convention, Program with Abstracts, v. 9, p. A23.

Campion, K. M., A. R. Sprague, D. Mohrig, R. W. Lovell, P. A. Drzewiecki, M. D. Sullivan, J. A. Ardill, G. N. Jensen, and D. K. Sickafoose, 2000, Outcrop expression of confined channel complexes, *in* P. Weimer, R. M. Slatt, J. Coleman, N. C. Rosen, H. Nelson, A. H. Bouma, M. J. Styzen, and D. T. Lawrence, eds., Deep water reservoirs of the world: Houston, Gulf Coast Section SEPM Foundation, p. 127–150.

Carter, R. M., and L. Carter, 1996, The abyssal Bounty fan and lower Bounty channel: evolution of a rifted-margin sedimentary system: Marine Geology, v. 130, p. 181–202.

Clark, J. D., and K. T. Pickering, 1996, Submarine channels processes and architecture: London, Vallis-Press, 231 p.

Hess, G. R., 1979, Miocene and Pliocene inner suprafan channel complex, San Clemente, California, *in* C. J. Stuart, ed., Guidebook to Miocene lithofacies and depositional environments, coastal southern California and northwestern Baja California: Pacific Section SEPM, p. 99–105.

Hiscott, R. N., F. R. Hall, and C. Pirmez, 1997a, Turbidity-current overspill from the Amazon channel: texture of the silt/sand load, paleoflow from anisotropy of magnetic susceptibility and implications for flow processes, *in* R. D. Flood, D. J. W. Piper, A. Klaus, and L. C. Peterson, eds., Proceedings of the Ocean Drilling Program, scientific results, v. 155: College Station, Texas, Ocean Drilling Program, p. 53–78.

Hiscott, R. N., K. T. Pickering, A. H. Bouma, B. M. Hand, B. C. Kneller, G. Postma, and W. Soh, 1997b, Basin floor fans in the North Sea: sequence stratigraphic model vs. sedimentary facies: discussion: AAPG Bulletin, v. 81, p. 662–665.

Ingle, J. C., 1971, Paleoecologic and paleobathymetric history of the late Miocene–Pliocene Capistrano Formation, Dana Point area, Orange County, California, *in* F. W. Bergen, ed., Geologic guide book Newport Lagoon to San Clemente, Orange County, California: coastal exposures of Miocene and early Pliocene rocks: Pacific Section SEPM, p. 71–88.

Kenyon, N. H., R. H. Belderson, and A. H. Stride, 1978, Channels, canyons and slump folds on the continental slope between south-west Ireland and Spain: Oceanologica Acta, v. 1, p. 369–380.

Kenyon, N. H., J. Millington, L. Droz, and M. K. Ivanov, 1995, Scour holes in a channel-lobe transition zone Rhone Cone, *in* K. T. Pickering, R. N. Hiscott, N. H. Kenyon, F. Ricci Lucchi, and R. D. A. Smith, eds., Atlas of deep water environments: architectural style in turbidite systems: London, Chapman and Hall, p. 212–215.

Kneller, B. C., and M. J. Branney, 1995, Sustained high density turbidity currents and the deposition of thick massive sands: Sedimentology, v. 42, p. 607–616.

Kneller, B., and C. Buckee, 2000, The structure and fluid mechanics of turbidity currents: a review of some recent studies and their geological implications, *in* J. L. Best, ed., Millennium reviews: Sedimentology, v. 47, p. 62–94.

Kneller, B. C., and W. D. McCaffrey, 1995, Modeling the effects of salt-induced topography on deposition from turbidity currents, *in* C. J. Travis, H. Harrison, M. R. Hudeac, B. C. Vendeville, F. J. Peel, and R. F. Perkins, eds., Salt, sediment and hydrocarbons: Gulf Coast Section SEPM, p. 137–145.

Lewis, K. B., 1971, Slumping on a continental slope inclined at 1°–4°: Sedimentology, v. 16, p. 97–110.

Marlow, M. S., J. V. Gardner, and W. R. Normark, 2000, Using high-resolution multibeam bathymetry to identify seafloor surface rupture along the Palos Verdes fault complex in offshore southern California: Geology, v. 28, p. 587–590.

Miall, A. D., 1985, Architectural-element analysis: a new method of facies analysis applied to fluvial deposits: Earth-Science Reviews, v. 22, p. 261–308.

Middleton, G. V., 1967, Experiments on density and turbidity currents: III. deposition of sediment: Canadian Journal of Earth Sciences, v. 4, p. 475–505.

Morris, W. R., and C. J. Busby-Spera, 1988, Sedimentological evolution of a submarine canyon in a forearc basin, Late Cretaceous Rosario Formation, San Carlos, Mexico: AAPG Bulletin, v. 72, p. 717–737.

Morris, W. R., and C. J. Busby-Spera, 1990, A submarine-fan valley-levee complex in the Upper Cretaceous Rosario Formation: implications for turbidites facies models: Geological Society of America Bulletin, v. 102, p. 900–914.

Mutti, E., and W. R. Normark, 1987, Comparing examples of modern and ancient turbidite systems: problems and concepts, *in* J. K. Leggett and G. G. Zuffa, eds., Marine clastic sedimentology: concepts and case studies: London, Graham and Trotman, p. 1–38.

Nilsen, T. H., H. Camacho, and T. W. Redin, 2000, Turbidite systems in California: Pacific Section Convention, AAPG Short Course Guide, unpaginated.

Normark, W. R., 1970, Growth patterns of deep-sea fans: AAPG Bulletin, v. 54, p. 2170–2195.

Shanmugam, G., 1996, High-density turbidity currents: are they sandy debris flows?: Journal of Sedimentary Research, v. 66, p. 2–10.

Vrolijk, P. J., and J. B. Southard, 1997, Experiments on rapid deposition of sand from high-velocity flows: Geoscience Canada, v. 24, p. 45–54.

Walker, R. G., 1975, Nested submarine-fan channels in the Capistrano Formation, San Clemente California: Geological Society of America Bulletin, v. 86, p. 915–924.

Weser, O. E., 1971, Proximal turbidite environment San Clemente State Park, *in* F. W. Bergen, ed., Geologic guide book Newport Lagoon to San Clemente, Orange County, California: coastal exposures of Miocene and early Pliocene rocks: Pacific Section SEPM, p. 55–70.